Modeling complex mechanical computer codes with functional input via Gaussian processes

Andrés F. López-Lopera[1,a], Franck Massa[1,b], Isabelle Turpin[1,a], Nicolas Leconte[2]

[1,a]*CERAMATHS, Univ. Polytechnique Hauts-de-France*
[1,b]*LAMIH, CNRS, UMR 8201, Univ. Polytechnique Hauts-de-France, INSA Hauts-de-France*
F-59313 Valenciennes, France
andres.lopezlopera@uphf.fr, isabelle.turpin@uphf.fr, franck.massa@uphf.fr
[2]*CRD, DMAS, ONERA*
F-59000 Lille, France
nicolas.leconte@onera.fr

Abstract. Surrogate models based on Gaussian processes (GPs) have been successfully used as a complement of costly-to-evaluate complex computer codes. They are capable to provide accurate predictions with confident intervals but require fewer costs (in both time and resources). Here, we focus on a class of mechanical codes with functional inputs and output force-displacement curves. We further investigate a GP framework where inputs are handled in a continuous setting, which results in more tractable and scalable models. Both input and output information are correlated using a composite kernel function that can be efficiently computed (and inverted) when tensor-structured data are considered. We demonstrate the reliability and scalability of the GP in a synthetic example with highly variable input and output curves, as well as on a real-world mechanical application modeling the self-piercing riveting (SPR) in a single hat component. Our experiments show that the methodology is able to correctly detect the maximum forces and the displacements at peak force where the failure of SPR appears.

Keywords: Surrogate models, Functional input data, Uncertainty quantification, Self-piercing riveting, Arcan test

1 Introduction

Mechanical system design involves different components which are connected with joints, such as bolts, rivets and pins. The complex behavior of these connecting elements plays a key role in the overall dynamic response of the assembly. A pure deterministic evaluation of the response can tend to conservative systems without addressing the crucial aspect of parameter uncertainties. To quantify them, experimental campaigns are performed to identify the material variability and repeatability of tests. For example, Weisz-Patrault et al. [1] quantified uncertainties resulting from the analysis of dynamic tests performed on a classic split Hopkinson pressure bar system to improve material parameter estimation via Bayesian inference. Doan et al. [2] focused on the geometrical variability in 3D lattice structures obtained by means of an Electron Beam Melting process. Estepa et al. [3] examined the evolution of mechanical properties and associated uncertainty for a set of rubber specimens after a thermal aging step.

The uncertainty propagation step can be numerically expensive with traditional sampling strategies when finite element models are considered to describe the studied system. To reduce cost but preserving accuracy, surrogate models have been widely studied in the mechanical engineering community. Among those models are Gaussian processes (GPs) which are fed by a statistically rich database of simulations generated by the mechanical code. They provide fast reliable predictions with confident intervals used for uncertainty quantification. Regression tasks (Sadet et al. [4]), uncertainty propagation (Denimal et al. [5]), reliability analysis (Li et al. [6]) and shape optimization (Gaudrie et al. [7]) are some of the topics where GPs have been successfully applied in mechanics.

In this paper, we focus on a class of mechanical codes where inputs are functional force-displacement curves. Since standard codes cannot handle inputs that are actually functions in a continuous setting, the latter are approximated by a parametric (and often simplistic) model. Then, the set of coefficients of the proxy model is passed as inputs to the code for a further analysis. Here, we instead seek to handle the inputs as nonparametric continuous functions for which no further approximations nor assumptions are required. In view of this, we suggest adapting the GP framework introduced by López-Lopera et al. [8] where kernel functions account for the functional input data. We must note that standard GPs may be contemplated considering a discrete representation of the inputs, or
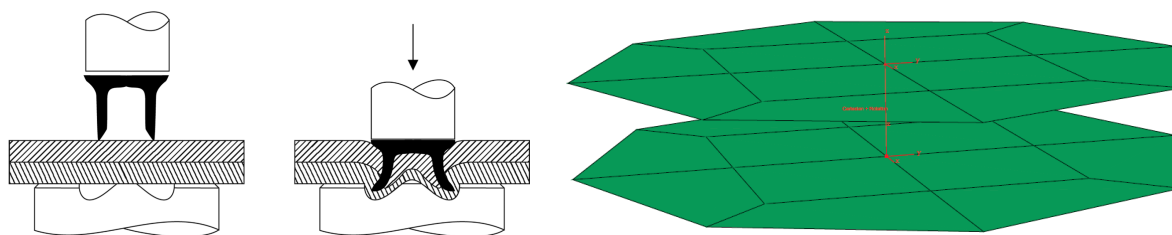
Figure 1. (left) Joining process of a self-piercing riveting (SPR) connection. (right) Joint numerical model.
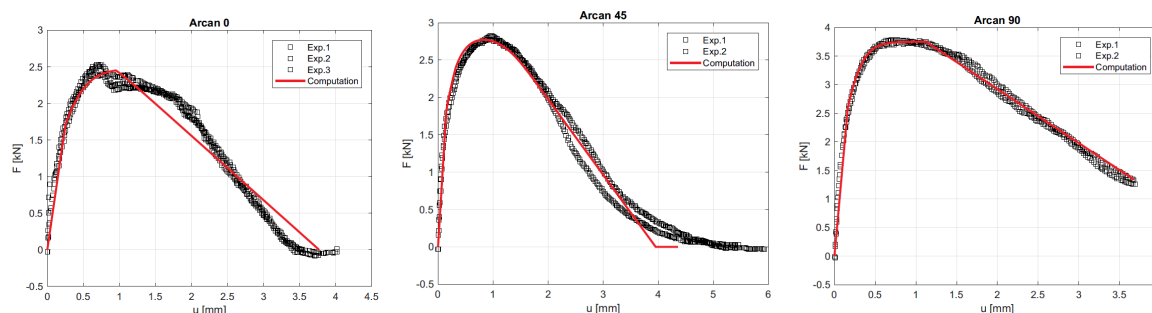

Figure 2. Force-displacement curves for Arcan tests: (left) pure tensile, (center) tensile/shear, and (right) pure shear. The panels show: the global force-displacement responses observed experimentally for the assembly (black points), and the parametric numerical responses of the joint model (red solid lines).

using the coefficients of the proxy model as inputs, but numerical implementations will quickly overload since kernels will be defined in high-dimensional Euclidean spaces. For instance, in the mechanical application in Section 2, inputs are of length 250 (number of discrete evaluations) and the proxy model depends on 13 parameters. In the functional case, since the kernel of the inputs is defined directly in the space of functions, the sizes of the covariance matrices remain smaller, and thus, the computation of GP predictions becomes more tractable and scalable. As in López-Lopera et al. [8], efficient numerical implementations result from the exploitation of tensor-structured data. Our methodology provides both predictions with confident intervals in the order of seconds, a significant computational improvement compared to the 4 hours required by the mechanical code.

The next sections are organized as follows. Section 2 describes the mechanical context. Section 3 establishes the GP framework with functional inputs. Section 4 contains the experiments of both a synthetic example and the mechanical application. Finally, section 5 summarizes the conclusions and future work.

2   Mechanical application

The SPR has been increasingly adopted in the industry as a high-speed mechanical fastening technique for the joining of sheet material, especially in the automotive industry where multi-material assembly has become a priority. The main interest comes from its capability to join a wide range of materials without requiring to make pre-drilled holes (Fig. 1, left panel).

To model point-to-point assemblies, a macro connector is considered based on 2-node generalized spring with three degrees of freedom in translation per node (Fig. 1, right panel). A 13-parameter proxy joint model is used featuring a linear elastic description, a Voce hardening law, a linear damage evolution, three β-norm criteria respectively used for the irreversible deformation threshold, the maximum force and the failure. The joint model is then calibrated with dynamic Arcan tests considering an aluminum/PA66 composite 2-sheet SPR assembly for three loading angles, namely pure tensile ($0°$), mixed tensile/shear ($45°$) and pure shear ($90°$). An example of both experimental and parametric force-displacement curves for Arcan tests are shown in Fig. 2. Next, the SPRs are integrated in a test component, described in Fig. 3 (left panel). Further details about the experimental setup, the modeling of the SPR and the numerical model of the single hat component are given in Leconte et al. [9]. Examples of experimental and numerical dynamic component tests are displayed in Fig. 3 (right panel).

It is known in the literature that the use of deterministic approaches are not sufficient to model a family of experimental results both for the Arcan tests and the test component. Indeed, the uncertainty associated to material properties, friction, and clamping force have been recently studied for SPR simulation model by Fang et al. [10] using machine learning methods. Here, we propose to link the force-displacement curves of a SPR (namely inputs) to the force-displacement curves of the test component (namely outputs) via GPs.
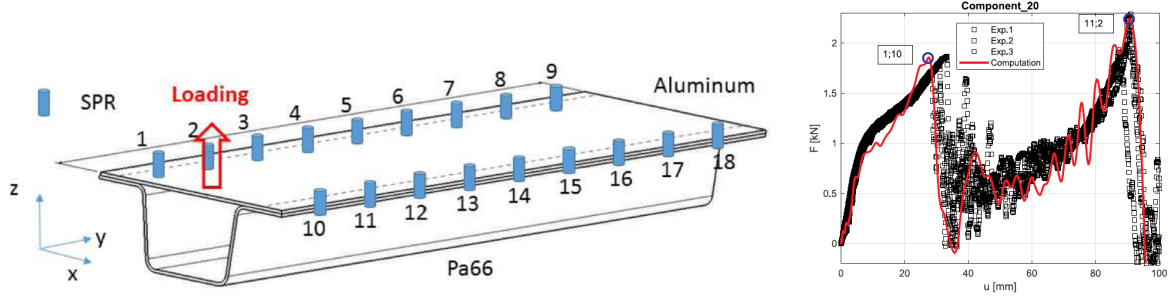
Figure 3. (left) Description of the single hat component made of an omega-shaped PA66 part assembled with a flat aluminum plate by 2 rows of 9 connectors. (right) An example of an experimental and numerical output force-displacement curves (black point and red solid line, respectively).

3 Gaussian process framework

Inline with the database in Section 4.2, we focus on functional inputs $f : \mathcal{T} \to \mathbb{R}$ with $\mathcal{T} \subseteq \mathbb{R}$. We establish the GP framework for a general cases with $q \in \mathbb{N}$ inputs. In our mechanical application, we only need to set $q = 3$. For clarity, we denote the displacement variables for the input and output curves as μ and u, respectively.

Let $\{Y(\boldsymbol{\mathcal{F}}, u); \boldsymbol{\mathcal{F}} \in \mathcal{F}(\mathcal{T}, \mathbb{R})^q, u \in \mathbb{R}\}$, with $\mathcal{F}(\mathcal{T}, \mathbb{R})$ the set of functions from $\mathcal{T}$ to $\mathbb{R}$, be a GP with functional inputs $\boldsymbol{\mathcal{F}} = (f_1, \ldots, f_q)$ and displacement u. The GP Y is completely defined by

$$Y \sim \mathcal{GP}(m, k),$$

where $m : \mathcal{C} \to \mathbb{R}$ and $k : \mathcal{C} \times \mathcal{C} \to \mathbb{R}$, with $\mathcal{C} := \mathcal{F}(\mathcal{T}, \mathbb{R})^q \times \mathbb{R}$, are the mean and covariance (namely kernel) functions. Here, we assume that $m(\cdot) = 0$ since data will be statistically learned by k. As suggested by López-Lopera et al. [8], a valid kernel accounting for both inputs $\boldsymbol{\mathcal{F}}$ and displacement u is given by the separable structure:

$$k((\boldsymbol{\mathcal{F}}, u), (\boldsymbol{\mathcal{F}}', u')) = k_f(\boldsymbol{\mathcal{F}}, \boldsymbol{\mathcal{F}}') k_u(u, u'), \tag{1}$$

with $k_f : \mathcal{F}(\mathcal{T}, \mathbb{R})^q \times \mathcal{F}(\mathcal{T}, \mathbb{R})^q \to \mathbb{R}$ and $k_u : \mathbb{R} \times \mathbb{R} \to \mathbb{R}$. We must note that, to avoid non-identifiability of the variance parameters, k_f is considered here as a correlation function, i.e. its variance parameter is equal to one.

Kernels for scalar variables are well known in the literature (see, e.g., Rasmussen and Williams [11]). An example of a stationary kernel k_u is the Matérn 5/2 kernel given by:

$$k_u(u, u') = \sigma^2 \left(1 + \sqrt{5}\frac{|u - u'|}{\ell_u} + \frac{5}{3}\frac{(u - u')^2}{\ell_u^2}\right) \exp\left\{-\sqrt{5}\frac{|u - u'|}{\ell_u}\right\}, \tag{2}$$

with σ^2 and ℓ_u the variance and length-scale parameters, respectively. While the former is seen as a scale parameter of the output, the latter is a scale for the input variable u. We refer to Rasmussen and Williams [11] for other stationary kernel structures. Next we focus on the construction of valid stationary kernels for functional inputs.

3.1 Construction of stationary kernels for functional inputs

To establish stationary kernels in the space of functions, we first need to define a distance between functions. As suggested by Betancourt et al. [12], we consider the L^2-norm as it leads to simpler and closed-form expressions:

$$d_{\boldsymbol{\ell}}(\boldsymbol{\mathcal{F}}, \boldsymbol{\mathcal{F}}') = \|\boldsymbol{\mathcal{F}} - \boldsymbol{\mathcal{F}}'\|_{\boldsymbol{\ell}}^2 = \sum_{i=1}^{q} \frac{\int_{\mathcal{T}} (f_i(\mu) - f_i'(\mu))^2 d\mu}{\ell_i^2}, \tag{3}$$

with length-scale parameters $\boldsymbol{\ell} = (\ell_1, \ldots, \ell_q) \in (0, \infty)^q$, and $\int_{\mathcal{T}} (f_i(\mu) - f_i'(\mu))^2 d\mu < \infty$ for $i = 1, \ldots, q$. Using eq. (3), we can now define stationary kernels for functional data, for instance, the Matérn 5/2 kernel:

$$k_f(\boldsymbol{\mathcal{F}}, \boldsymbol{\mathcal{F}}') = \left(1 + \sqrt{5}\|\boldsymbol{\mathcal{F}} - \boldsymbol{\mathcal{F}}'\|_{\boldsymbol{\ell}} + \frac{5}{3}\|\boldsymbol{\mathcal{F}} - \boldsymbol{\mathcal{F}}'\|_{\boldsymbol{\ell}}^2\right) \exp\left\{-\sqrt{5}\|\boldsymbol{\mathcal{F}} - \boldsymbol{\mathcal{F}}'\|_{\boldsymbol{\ell}}\right\}. \tag{4}$$

The computation of eq. (3) relies on the tractability of the q integrals. In our application, the functional forms of f_i and f_i' are actually unknown, and thus, integrals cannot be computed. In this case, both f_i and f_i' need to be replaced by linear approximations where the integrals operate on basis functions in which the resulting Gram matrix is computable. As discussed in Betancourt et al. [12], the integrals in eq. (3) have closed-form expressions for approximations based on splines or PCA. We refer to López-Lopera et al. [8] for a further discussion on other stationary kernel structures for functional data and the computation of the L^2-norm using linear approximations.

3.2 Gaussian process predictions

One of the main benefits of GPs relies in the tractability of conditional distributions. Without loss of generality, we consider N_r responses observed at displacements $u_1, \ldots, u_{N_u}$. Consider conditioning Y to an observation vector $\boldsymbol{y}_N = [y_{1,1}, \ldots, y_{1,N_u}, \ldots, y_{N_r,N_u}]^\top$ evaluated at tuples $((\boldsymbol{\mathcal{F}}_1, u_1), \ldots, (\boldsymbol{\mathcal{F}}_1, u_{N_u}), \ldots, (\boldsymbol{\mathcal{F}}_{N_r}, u_{N_u}))$. The conditional distribution $Y|\{\mathbf{Y}_N = \boldsymbol{y}_N\}$, with $\mathbf{Y}_N = [Y(\boldsymbol{\mathcal{F}}_1, u_1), \ldots, Y(\boldsymbol{\mathcal{F}}_1, u_{N_u}), \ldots, Y(\boldsymbol{\mathcal{F}}_{N_r}, u_{N_u})]^\top$, is then Gaussian-distributed with conditional mean function m_c and conditional covariance function c given by

$$m_c(\boldsymbol{\mathcal{F}}_*, u_*) = \boldsymbol{k}^\top(\boldsymbol{\mathcal{F}}_*, u_*)\mathbf{K}^{-1}\boldsymbol{y}_N,$$

$$c((\boldsymbol{\mathcal{F}}_*, u_*), (\boldsymbol{\mathcal{F}}'_*, u'_*)) = k((\boldsymbol{\mathcal{F}}_*, u_*), (\boldsymbol{\mathcal{F}}'_*, u'_*)) - \boldsymbol{k}^\top(\boldsymbol{\mathcal{F}}_*, u_*)\mathbf{K}^{-1}\boldsymbol{k}(\boldsymbol{\mathcal{F}}'_*, u'_*),$$

with covariance matrix $\mathbf{K} = (k((\boldsymbol{\mathcal{F}}_i, u_j), (\boldsymbol{\mathcal{F}}_{i'}, u_{j'})))_{1 \le i, i' \le N_r, 1 \le j, j' \le N_u}$ and cross-covariance vector $\boldsymbol{k}(\boldsymbol{\mathcal{F}}, u) = [k((\boldsymbol{\mathcal{F}}, u), (\boldsymbol{\mathcal{F}}_1, u_1)), \ldots, k((\boldsymbol{\mathcal{F}}, u), (\boldsymbol{\mathcal{F}}_1, u_{N_u})), \ldots, k((\boldsymbol{\mathcal{F}}, u), (\boldsymbol{\mathcal{F}}_{N_r}, u_{N_u}))]^\top$. The mean evaluation $m_c(\boldsymbol{\mathcal{F}}_*, u_*)$ is used as a point estimate of $Y(\boldsymbol{\mathcal{F}}_*, u_*)$, and the variance $v(\boldsymbol{\mathcal{F}}_*, u_*) = c((\boldsymbol{\mathcal{F}}_*, u_*), (\boldsymbol{\mathcal{F}}_*, u_*))$ is used as the expected square error of this estimate. For fitting the GP to observations $\boldsymbol{y}_N$, the covariance parameters $\boldsymbol{\theta} = (\sigma^2, \ell_u, \ell_1, \ell_2, \ell_3)$ are estimated by maximizing the log-likelihood (see, e.g., Rasmussen and Williams [11]).

Remark: Computational complexity. The complexity of the GP relies on the inversion of $\mathbf{K}$ which is $\mathcal{O}(N_r^3 N_u^3)$. It can be reduced to $\mathcal{O}(N_r^3) + \mathcal{O}(N_u^3)$ by considering Kronecker implementations of the kernel in eq. (1).

4 Numerical experiments

Implementations here are based on the R package `kergp` (Deville et al. [13]), and experiments are executed on an 11th Gen Intel(R) Core(TM) i5-1145G7 2.60GHz 1.50 GHz, 16 Gb RAM. Both R codes and notebooks to reproduce some of the experiments are available in the Github repository: `https://github.com/anfelopera/spatfGPs`. For numerical stability reasons, we consider Matérn 5/2 kernels (see eqs. (2) and (4)) where the covariance parameters $\boldsymbol{\theta} = (\sigma^2, \ell_u, \ell_1, \ell_2, \ell_3)$ are estimated via maximum likelihood.

In our implementations, we focus on PCA approximations of the inputs since they lead to two main computational benefits. First, the Gram matrix of the basis functions is an identity matrix due to orthonormality properties. Second, the most relevant information from inputs can be encoded in a few amount of principal components. We consider a PCA approximation seeking to ensure a total inertia of 99.99% for the representation of the inputs in Fig. 6. This leads to $\boldsymbol{p} = (5, 10, 5)$ with p_i the number of principal components for the i-th functional input.

We compare the quality of predictions in terms of the Q^2 criterion on unobserved data which is defined as:

$$Q^2 = 1 - \frac{\sum_{i=1}^{n_{\text{test}}}(y_i - \widehat{y}_i)^2}{\sum_{i=1}^{n_{\text{test}}}(y_i - \overline{y})^2},$$

where $(y_1, \ldots, y_{n_{\text{test}}})$ is the set of test observations, $(\widehat{y}_1, \ldots, \widehat{y}_{n_{\text{test}}})$ the set of the corresponding GP predictions and $\overline{y} = \frac{1}{n_{\text{test}}}\sum_{i=1}^{n_{\text{test}}} y_i$. For the noise-free case, the Q^2 criterion is equal to one if predictions are exactly equal to the test data, equal to zero if they are equal to the constant prediction $\overline{y}$, and lower if they perform worse than $\overline{y}$.

4.1 Influence of the number of training scenarios

We first analyze a synthetic example to assess the influence of the number of training scenarios in the performance of the GP framework. As in the mechanical application, we consider $q = 3$ inputs and one output.

Generation of the input and output curves. We consider as functional inputs, for $i = 1, 2, 3$ and $\mu \in [0, 1]$:

$$f_i(\mu) = \frac{s \cdot r_\rho(\mu)}{\max(r_\rho(\mu))},$$

with $r_\rho(\mu) = \frac{\mu}{\rho^2}e^{-\mu^2/2\rho^2}$ the Rayleigh probability density function, $\rho \sim \text{Uniform}(0.05, 1)$ a shape parameter, and $s \sim \text{Uniform}(2, 4)$ a scale parameter. This setup is chosen to emulate the input curves in Fig. 2 but seeking greater variability. We generate 500 random replicates for each input (Fig. 4, left panels). The corresponding output of each input replicate is generated using a GP with $\boldsymbol{\theta}_\star = (\sigma^2 = 1, \ell_u = 0.04, \ell_1 = 20, \ell_2 = 20, \ell_3 = 20)$. This choice is made seeking a high variability of the output while retaining an identifiable functional form (see Fig. 4, right panel). The inputs and outputs are evaluated at 100 and 50 discrete equispaced displacement values, respectively. For the inputs, we perform a PCA approximation ensuring a total inertia of 99.9% leading to $\boldsymbol{p} = (5, 6, 5)$.
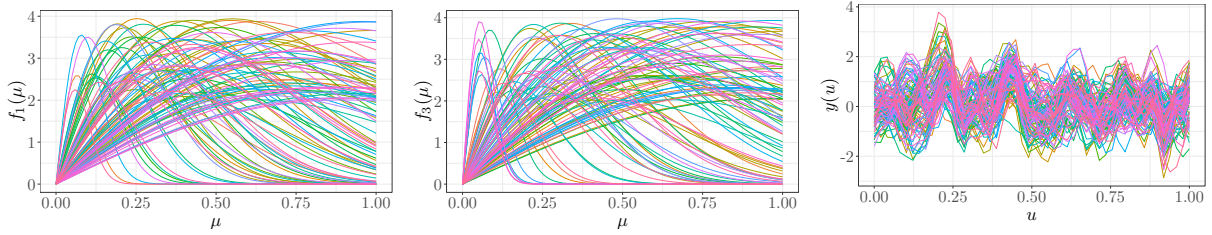
Figure 4. Replicates of (left) the first and third functional inputs and (right) the outputs generated in Section 4.1.
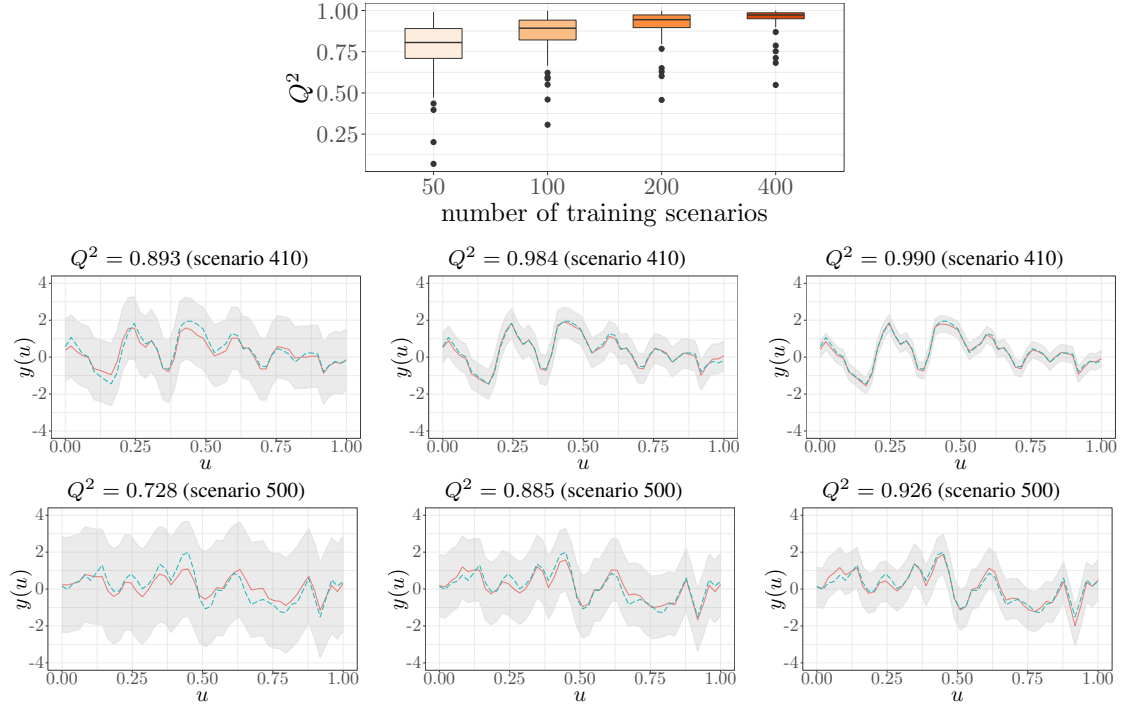

Figure 5. (top) Q^2 results considering different training sets with $n_{\text{train}} = 50, 100, 200, 400$. Boxplots are computed over the 100 test scenarios. (bottom) GP predictions of scenarios (from top to bottom) 410 and 500 with (from left to right) $n_{\text{train}} = 50, 200, 400$. The panels show: (dashed blue line) the target function, (solid red line) the GP mean prediction and (gray regions) 3-standard deviation confidence intervals.

Cross-validation test. To test the GP framework, we split the database into a training set and a test set. The first 400 scenarios are kept for training the GP model and the other 100 are used for prediction testing. We train models considering different sizes of training sets, with $n_{\text{train}} = 50, 100, 400$, to numerically test the convergence of GP predictions. Those models are initialized with $\boldsymbol{\theta}_0 = (\sigma^2 = 1, \ell_u = 0.1, \ell_1 = 10, \ell_2 = 10, \ell_3 = 10)$.

Figure 5 shows boxplots of the Q^2 values and two examples of GP predictions. It is observed that, as the number of training scenarios increases, predictions are more accurate (with Q^2 median values closer to one), and that confidence intervals are thinner. This allows to conclude that, with a sufficiently rich training set, the GP framework is able to capture the output dynamics while providing confident intervals.

4.2 Mechanical application

Database. The numerical joint and hat component models are respectively used to build the input and output force-displacement curves. The inputs are parameterized with 13 material parameters (see [9]). To explore the associated input design space, a Latin-hypercupe sampling (LHS) is used to independently generate 100 snapshots (namely scenarios). The computational cost is about 4 hours per sample by considering an Abaqus/explicit integration method evaluated at 250 and 8585 discrete input and output displacements, respectively. After a post-processing step applied to filter out repeated evaluations and to reduce the resolution of the responses, output curves become of length 791. Figure 6 (top panels) shows the replicates of the first and second input curves and the outputs.

Leave-one-out (LOO) test. We here assess the GP framework via an LOO cross-validation test, i.e. each scenario
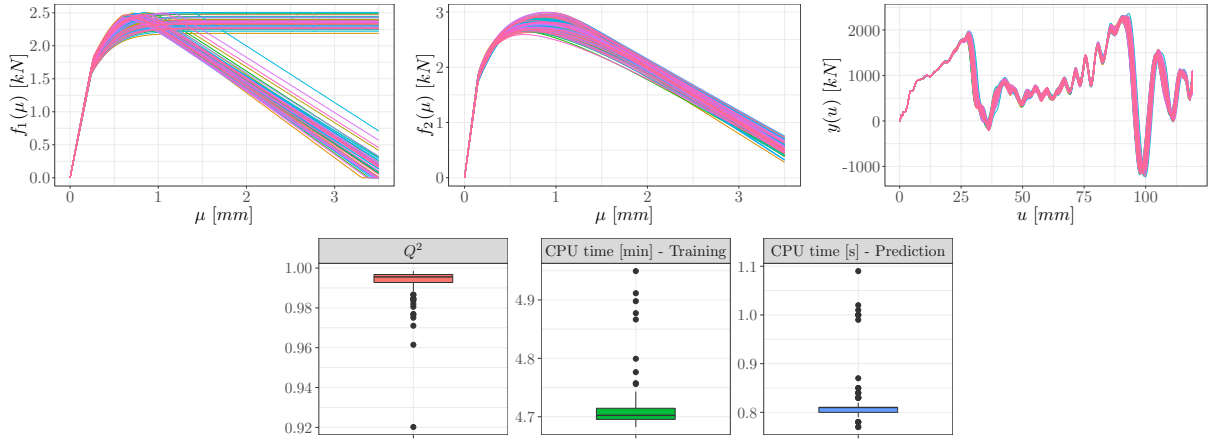
Figure 6. (top) Replicates of the first and second inputs and the outputs of the mechanical database. (bottom) Boxplots of performance indicators considering the 100 LOO tests proposed in Section 4.2.
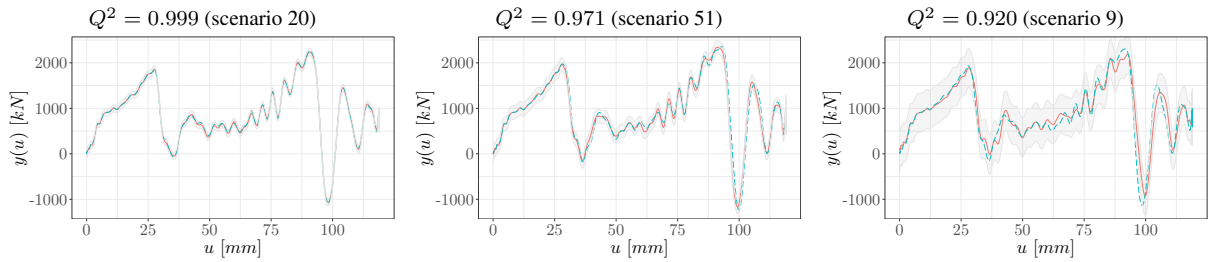

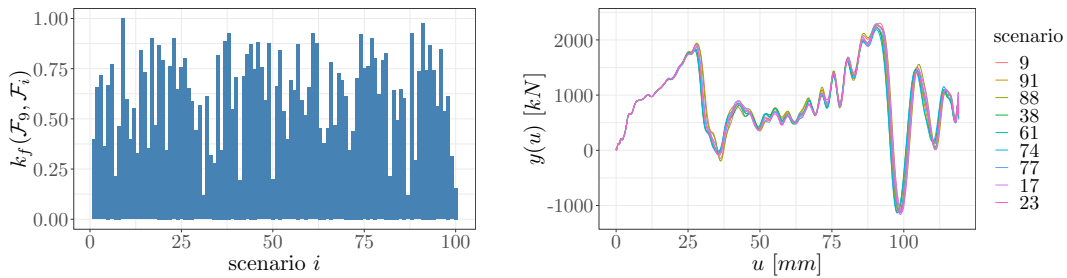Figure 7. Examples of GP predictions of the output force-displacement curves. The panel description is as in Fig. 5.

Figure 8. Additional results for the scenario 9. The panels show: (left) the correlation values $k_f(\mathcal{F}_9, \mathcal{F}_i)$ for $i = 1, \ldots, 100$, and (right) the output curves of the scenarios leading to $k_f(\mathcal{F}_9, \mathcal{F}_i) > 0.9$.

is predicted at a time using a GP trained with a reduced database that does not include data from the scenario of interest. This results in 100 independent models that are initialized with $\ell_u = 1 \times 10^{-3}, \ell_1 = 10, \ell_2 = 10, \ell_3 = 10$, and with a variance parameter σ^2 equal to 5% of the variance of the output. These parameters are optimized by performing a maximum likelihood estimation routine with 1×10^3 iterations.

Figure 6 shows that the GP models provide values of $Q^2 > 0.92$ in less than 5 min (including both training and prediction steps), a significant computational improvement compared to the 4 hours required by the mechanical code. From Fig. 7, we note that, in addition to providing accurate predictions, models also lead to confidence intervals that are thinner as the model is trustworthy, and wider when they are less reliable (see predictions of scenarios 20 and 9, respectively). We also observe that the maximum output force peaks are correctly predicted, which is crucial for detecting the displacement values where the failures of SPR appear.

Figures 6 and 7 show that the scenario 9 was more challenging to predict. After checking the values of $k_f(\mathcal{F}_9, \mathcal{F}_i)$, for $i \in \{1, \ldots, 100\} \backslash 9$ (see Fig. 8), we have noted that this scenario was predominantly matched to others with distinct input and output curves, which explains the inaccurate prediction issue with wide confidence intervals. As discussed by López-Lopera et al. [8], this occurs when the training set does not contain scenarios "similar" to the test one. Since the 100 scenarios have been selected via LHS promoting input space filling, it was already expected to have "unique" scenarios in the database, and thus difficult to predict in an exhaustive LOO test. In practice, the GP is used to predict outputs associated to new inputs contained in the input domain covered by the training set. In that case, and according to our experiments, we expect it to provide reliable predictions often.

5 Conclusions

We further investigate a GP framework with functional inputs. It has the particularity of handling the inputs in a continuous setting, which is not possible with other approaches from the state-of-the-art. We test the performance and scalability of the GP on a synthetic example with highly variable curves, as well as on a real-world application describing the behavior of SPR subject to material variability. Once the GP is trained, it is able to provide accurate predictions with confidence intervals in less than a second. Our experiments show that the methodology is capable to correctly detect the maximum forces and the displacements at peak force where the failure of a rivet line appears.

After the numerical tests, we have noticed that the GP framework deserves to be tested on peak forces at more distinct displacement values. To do so, a further analysis of the input space, for instance the 13-dimensional input space of the joint model, will be required to achieve greater variability in the outputs. We expect that these new output curves may be more challenging to predict and that the training set needs to be enriched with more than a hundred scenarios. In that case, since the computational cost of the GP can be overheated, complexity reduction techniques may be applied to the outputs (e.g., a Fourier decomposition).

Authorship statement. The authors hereby confirm that they are the sole liable persons responsible for the authorship of this work, and that all material that has been herein included as part of the present paper is either the property (and authorship) of the authors, or has the permission of the owners to be included here.

References

[1] D. Weisz-Patrault, C. Francart, and G. Seisson. Uncertainty estimation and hierarchical Bayesian analysis of mechanical dynamic tests. Journal of Dynamic Behavior of Materials, vol. 7, n. 3, pp. 447–468, 2021.

[2] V. Doan, F. Massa, T. Tison, and H. Naceur. Coupling of homotopy perturbation method and Kriging surrogate model for an efficient fuzzy linear buckling analysis: Application to additively manufactured lattice structures. Applied Mathematical Modelling, vol. 97, pp. 602–618, 2021.

[3] A. M. Estepa, F. Massa, A. Boukamel, T. Tison, P. Champagne, S. Méo, and A. Wolf. Experimental and numerical investigations for quantifying variability of NR mechanical properties after thermal aging. Rubber Chemistry and Technology, vol. 94, n. 1, pp. 160–179, 2020.

[4] J. Sadet, F. Massa, T. Tison, E. Talbi, and I. Turpin. Deep Gaussian process for the approximation of a quadratic eigenvalue problem: Application to friction-induced vibration. Vibration, vol. 5, n. 2, pp. 344–369, 2022.

[5] E. Denimal, J. Sinou, and S. Nacivet. Prediction of squeal instabilities of a finite element model automotive brake with uncertain structural and environmental parameters with a hybrid surrogate model. Journal of Vibration and Acoustics, vol. 144, n. 2, pp. 021006, 2021.

[6] M. Li, M. Sadoughi, Z. Hu, and C. Hu. A hybrid Gaussian process model for system reliability analysis. Reliability Engineering & System Safety, vol. 197, pp. 106816, 2020.

[7] D. Gaudrie, R. Le Riche, V. Picheny, B. Enaux, and V. Herbert. Modeling and optimization with Gaussian processes in reduced eigenbases. Structural and Multidisciplinary Optimization, vol. 61, pp. 2343–2361, 2020.

[8] A. F. López-Lopera, D. Idier, J. Rohmer, and Bachoc. Multioutput Gaussian processes with functional data: A study on coastal flood hazard assessment. Reliability Engineering & System Safety, vol. 218, pp. 108139, 2022.

[9] N. Leconte, B. Bourel, F. Lauro, C. Badulescu, and E. Markiewicz. Strength and failure of an aluminum/PA66 self-piercing riveted assembly at low and moderate loading rates: Experiments and modeling. International Journal of Impact Engineering, vol. 142, pp. 103587, 2020.

[10] Y. Fang, L. Huang, Z. Zhan, S. Huang, and W. Han. Effect analysis for the uncertain parameters on self-piercing riveting simulation model using machine learning model. In WCX SAE World Congress Experience. SAE International, 2020.

[11] C. E. Rasmussen and C. K. I. Williams. Gaussian processes for machine learning (adaptive computation and machine learning). The MIT Press, Cambridge, MA, 2005.

[12] J. Betancourt, F. Bachoc, T. Klein, D. Idier, R. Pedreros, and J. Rohmer. Gaussian process metamodeling of functional-input code for coastal flood hazard assessment. Reliability Engineering & System Safety, vol. 198, pp. 106870, 2020.

[13] Y. Deville, D. Ginsbourger, and O. Roustant. kergp: Gaussian process laboratory (0.5.0). R package, 2019.